

Article

Thermodynamic Performance Analyses and Optimization of Dual-Loop Organic Rankine Cycles for Internal Combustion Engine Waste Heat Recovery

Zhong Ge ^{1,2}, Jian Li ², Yuanyuan Duan ^{2,*}, Zhen Yang ² and Zhiyong Xie ¹

¹ School of Architecture and Urban Planning, Yunnan University, Kunming 650500, China; zhongge@hotmail.com (Z.G.); xiezhiyong@ynu.edu.cn (Z.X.)

² Key Laboratory for Thermal Science and Power Engineering of MOE, Beijing Key Laboratory for CO₂ Utilization and Reduction Technology, Tsinghua University, Beijing 100084, China; jian-li15@mails.tsinghua.edu.cn (J.L.); zhenyang@tsinghua.edu.cn (Z.Y.)

* Correspondence: yyduan@tsinghua.edu.cn

Received: 3 January 2019; Accepted: 12 February 2019; Published: 16 February 2019



Featured Application: This work examined the effects of an internal combustion engine (ICE) exhaust gas temperature on dual-loop organic Rankine cycles (DORC) for ICE waste heat recovery. High-temperature loop evaporation, condensation temperatures, and superheat degrees were optimized. Results could provide theoretical and data support for determining suitable operating parameters and working fluid for DORC with various engine exhaust gas temperatures.

Abstract: Waste heats of an internal combustion engine (ICE) are recovered by a dual-loop organic Rankine cycle (DORC). Thermodynamic performance analyses and optimizations are conducted with 523.15–623.15 K exhaust gas temperature (T_{g1}). Cyclopentane, cyclohexane, benzene, and toluene are selected as working fluids for high-temperature loop (HTL), whereas R1234ze(E), R600a, R245fa, and R601a are selected as working fluids for low-temperature loop (LTL). The HTL evaporation temperature, condensation temperature, and superheat degree are optimized through a genetic algorithm, and net power output is selected as the objective function. Influences of T_{g1} on system net power output, thermal efficiency, exergy efficiency, HTL evaporation temperature, HTL condensation temperature, HTL superheat degree, exhaust gas temperature at the exit of the HTL evaporator, heat utilization ratio, and exergy destruction rate of the components are analyzed. Results are presented as follows: the net power output is mainly influenced by HTL working fluid. The optimal LTL working fluid is R1234ze(E). The optimal HTL evaporator temperature increases with T_{g1} until it reaches the upper limit. The optimal HTL condensation temperature increases initially and later remains unchanged for a cyclopentane system, thus keeping constant for other systems. Saturated cycle is suitable for cyclohexane, benzene, and toluene systems. Superheat cycle improves the net power output for a cyclopentane system when T_{g1} is 568.15–623.15 K.

Keywords: dual-loop organic Rankine cycle; waste heat recovery; performance analysis; parametric optimization; exhaust gas temperature

1. Introduction

Increased fossil fuel consumption causes environmental pollution, global warming, and energy crisis; waste heat recovery is considered a promising technology for solving these problems [1–3]. The waste heat utilization of internal combustion engine (ICE) can effectively reduce the use of fossil fuels and is crucial for saving energy and reducing emission because oils consumed by ICE account for

approximately 60% of the total oil consumption, and more than 55% of fuel energy is emitted through waste heat [4–7].

Among all of the existing solutions for the waste heat utilization of ICE, organic Rankine cycle (ORC) is a promising technology. ORC uses organic working fluids; this technology has advantages of simple structure, favorable applicability, and user-friendliness over conventional steam Rankine cycle and is ideal for utilizing medium-to-low temperature heat sources (<350 °C) [8–11]. Many researchers have conducted studies on ICE waste heat recovery using ORC and have discovered the favorable potential of this technology [12–18]. Shu et al. [12] used ORC to recover waste heat of diesel engine using alkanes as working fluids. Their results showed that cyclohexane and cyclopentane are the most suitable working fluids through comprehensive consideration. Vaja et al. [13] performed a thermodynamic analysis of ICE waste heat recovery using ORC, benzene, R11, and R134a as working fluids and considered different cycle configurations. Their results indicated that the overall efficiency of ORC is better by 12% than when ORC is not applied. Song et al. [17] designed an optimized ORC for marine diesel engine waste heat recovery and conducted economic and off-design analyses. Their results demonstrated that an optimized ORC is technically feasible and economically attractive.

ICE waste heat resources mainly consist of engine exhaust and jacket cooling water; given the high temperature of engine exhaust gas when a single-stage ORC is applied for waste heat recovery, the match between an engine exhaust gas and a high-temperature loop (HTL) may exacerbate, and the utilization of engine jacket cooling water is low [19,20]. Therefore, many researchers have adopted a dual-loop organic Rankine cycle (DORC) for ICE waste heat recovery and conducted system analysis, parametric analysis, and configuration comparison. Shu et al. [21–23] designed several systems for utilizing the ICE waste heat. Their results showed that R143a and R1234yf are favorable working fluids for low-temperature loop (LTL), and low condensation temperature can improve system performance. Tian et al. [19] investigated a regenerative transcritical system for ICE waste heat recovery. Their results showed that toluene is a favorable option for HTLs. Zhang et al. [24] developed a novel DORC to recover waste heat from exhaust gas, intake air, and coolant. Their results indicated that DORC can relatively improve output power by 14–16% in the peak of the effective thermal efficiency region. Yang et al. [25] studied a DORC for diesel engine waste heat recovery under various operating conditions; these authors selected R245fa as the working fluid and discussed performance on the basis of the first and second laws of thermodynamics. Their conclusion revealed that DORC can enhance the system thermal efficiency by 13% in comparison with the original system. Wang et al. [26,27] used DORC to harness the wasted heat from ICE and calculated the performance of a combined engine–ORC system under the entire operating region of an engine. Their results indicated that the relative increment rate of net power output can reach 22% in the peak thermal efficiency region. Choi and Kim [28] investigated a DORC waste heat recovery system, used water and R1234yf for HTLs and LTLs, and analyzed the thermodynamic properties of a waste heat recovery power generation system. Their results showed that the DORC can enhance 2.824% propulsion efficiency in comparison with the original engine. Song et al. [29,30] conducted a parametric analysis of the DORC system; these authors selected cyclohexane, toluene, and water as working fluids for HTLs, and used R245fa, R236fa, and R123 for LTLs. Their conclusion showed that the DORC can increase the net power output by 11.6% in comparison with an original diesel engine. A few researchers have conducted parameter optimization for DORCs. Yang et al. [31] explored DORC parameter optimization using R245fa for maximizing net power output and minimizing heat transfer area and used optimization parameters, such as evaporation pressure, superheat degree, and condensation temperature. Their results indicated that the maximum net power output can reach 23.62 kW.

Considering that exhaust gas is the main heat source of ICE waste heat, the exhaust gas temperature will considerably affect the working fluid selection for the two loops, the system thermal performance, and the operating parameters. Many works on the DORC have been based on fixed exhaust gas temperature, and a few studies have discussed the influence of exhaust gas temperature on the working fluid selection for two loops. In addition, HTL evaporation temperature, condensation

temperature and superheat degree are important operation parameters. Many studies have been conducted using a saturated cycle or fixed HTL condensation temperature, but a few studies have considered these operational parameters together for different working fluid systems. The change in engine exhaust gas temperature will affect the exergy destruction rate, and thus this change must be analyzed.

The engine exhaust gas temperatures of 523.15–623.15 K are considered in the present work because these temperatures are common and suitable for ORC application [6,29,30]. Cyclopentane, cyclohexane, benzene, and toluene [12,18,29,32–36] are selected as the HTL working fluids because they possess efficient thermal performance with high temperature and favorable environmental and high decomposition temperature. Furthermore, R1234ze(E), R600a, R245fa, and R601a are selected as working fluids for LTLs [8,37–41] given the efficient environmental and thermal performances with low temperature. The working fluid properties are listed in Table 1 [8,12,29,38], ODP is the ozone depletion potential; GWP is the global warming potential.

Table 1. Working fluids properties. ODP: ozone depletion potential; GWP: global warming potential.

	Molecular Mass/(g·mol ⁻¹)	Critical Temperature/K	Critical Pressure/kPa	Normal Boiling Point/K	ODP	GWP
cyclopentane	70.13	511.7	4515	322.4	0	low
cyclohexane	84.16	553.6	4075	353.9	0	low
benzene	78.11	562.1	4894	353.2	0	low
toluene	92.14	591.8	4126	383.8	0	low
R1234ze(E)	114.04	382.5	3636	254.2	0	6
R600a	58.12	407.8	3629	261.4	0	low
R245fa	134.05	427.2	3651	288.3	0	950
R601a	72.15	460.4	3378	301.0	0	low

By considering the exhaust gas acid dew point temperature limit, the present work optimizes HTL evaporation temperature, condensation temperature and superheat degree for maximizing net power output with 523.15–623.15 K engine exhaust gas through a genetic algorithm. Moreover, the effects of ICE exhaust gas temperature on net power output, thermal efficiency, exergy efficiency, HTL evaporation temperature, HTL condensation temperature, HTL superheat degree, exhaust gas temperature at the exit of an HTL evaporator, heat utilization ratio and exergy destruction rate of the components are studied.

2. System Model

A schematic of the DORC is illustrated in Figure 1. The DORC consists of an HTL and an LTL. The HTL is used to recover the waste heat of engine exhaust gas, and the LTL absorbs the heat of the jacket cooling water and released by HTL.

For HTL: An HTL working fluid pump pressurizes saturated liquid from a condenser/evaporator to an HTL evaporation pressure (1–2). The high-pressure liquid absorbs heat from an engine exhaust gas in the HTL evaporator and is heated to a saturated or superheat vapor (2–5). The saturated or superheated vapor from the HTL evaporator enters the HTL turbine and expands to perform work (5–6). The exhaust vapor exits from the HTL turbine and then enters the condenser/evaporator to release heat to the LTL (6–1).

For LTL: An LTL working fluid pump pressurizes saturated liquid from an LTL condenser to an LTL evaporation pressure (1'–2'). The liquid from the LTL working fluid pump enters an LTL preheater and absorbs heat to preheating (2'–7'), and then working fluid enters the condenser/evaporator and absorbs heat for evaporating (7'–4'). Working fluid with a saturated state enters the LTL turbine and generates power (4'–5'). The exhaust vapor enters the LTL condenser and condenses to a liquid (5'–1').

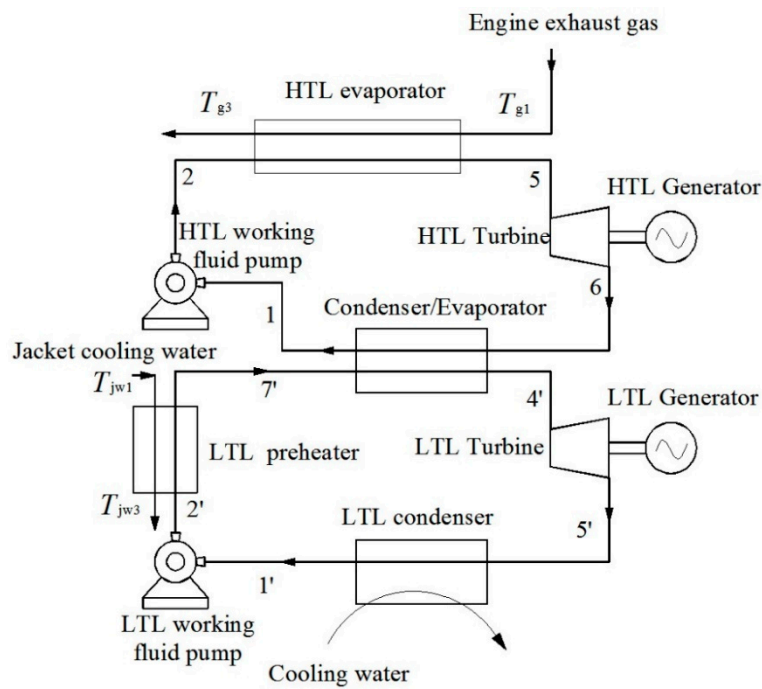


Figure 1. Schematic of the studied dual-loop organic Rankine cycle (DORC) system.

2.1. High-Temperature Loop

The T - s diagram of an HTL is depicted in Figure 2. Two cases for a pinch point temperature difference (PPTD) position of the HTL evaporator are observed. When the PPTD of the HTL evaporator is at an HTL working fluid evaporation bubble point (State point 3, VPP) [8], the HTL mass flow rate is calculated as follows:

$$m_H = \frac{m_g c_{pg} (T_{g1} - T_{g2})}{(h_5 - h_3)} \quad (1)$$

$$h_5 = f(p_{He}, T_5) \quad (2)$$

where h is the specific enthalpy; m_g is the mass flow rate of the engine exhaust gas; c_{pg} is the specific heat capacity of the engine exhaust gas at constant pressure, which is set to 1.1 kJ/(kg·K) [42]; T_g is the engine exhaust gas temperature; and p_{He} is the HTL evaporation pressure.

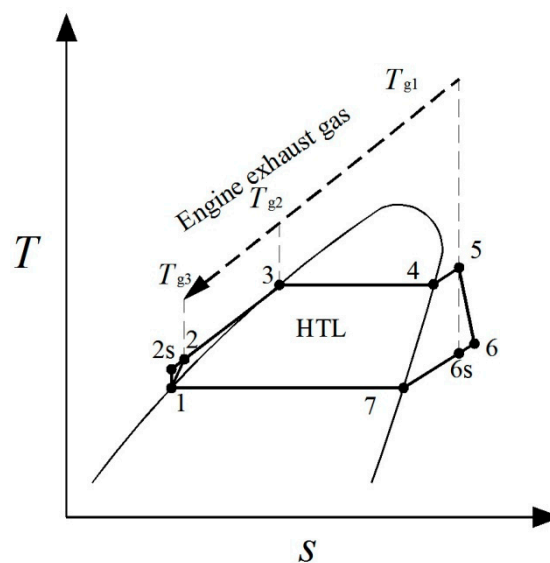


Figure 2. High-temperature loop (HTL) T - s diagram.

When the PPTD is at the working fluid inlet (State point 2, PPP), the HTL mass flow rate is calculated as follows:

$$m_H = \frac{m_g c_{pg} (T_{g1} - T_{g3})}{(h_5 - h_2)} \tag{3}$$

$$T_{g3} = T_2 + \Delta T_{pp1} \tag{4}$$

The power produced by the HTL turbine can be expressed as follows:

$$P_H = m_H (h_5 - h_{6s}) \eta_t = m_H (h_5 - h_6) \tag{5}$$

where η_t is the turbine isentropic efficiency.

The power consumed by the HTL working fluid pump can be calculated as follows:

$$P_{Hp} = \frac{m_H (h_{2s} - h_1)}{\eta_p} = m_H (h_2 - h_1) \tag{6}$$

where η_p is the working fluid pump efficiency.

The HTL net power output is equal to the power produced by the HTL turbine minus the power consumed by the HTL working fluid pump.

$$P_{Hnet} = P_H - P_{Hp} \tag{7}$$

2.2. Low-Temperature Loop

In Figure 3, two cases are identified for the LTL. If $T_{3'} + T_{pp2} \leq T_{jw1}$, then Case 1 occurs. In Figure 3a, the LTL working fluid is preheated by the jacket cooling water to a two-phase state.

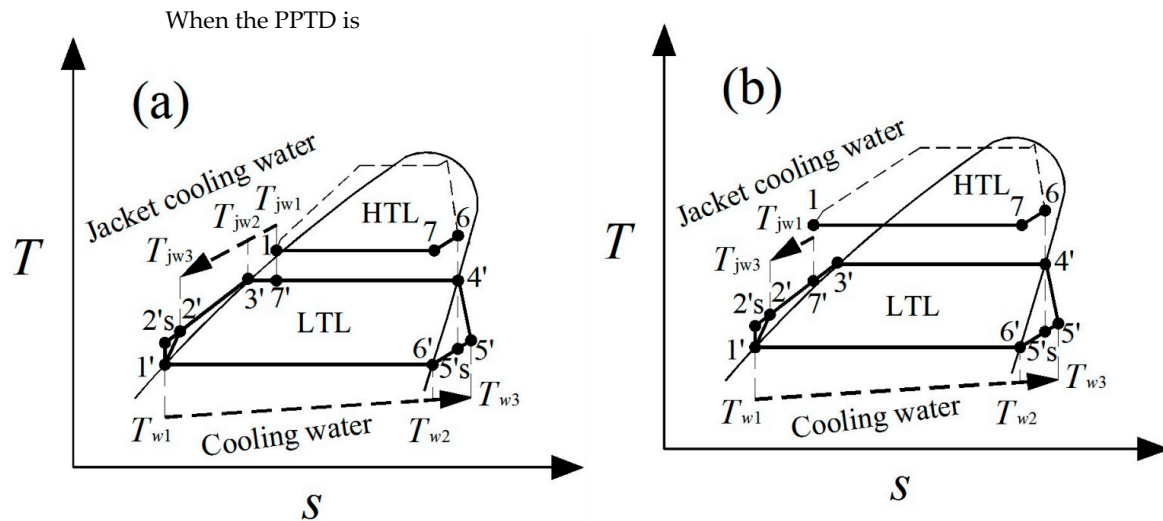


Figure 3. Low-temperature loop (LTL) T-s diagram: (a) Case 1 ($T_{3'} + T_{pp2} \leq T_{jw1}$); (b) Case 2 ($T_{3'} + T_{pp2} > T_{jw1}$).

When the PPTD of an LTL preheater is at State point 3', the LTL working fluid mass flow rate can be expressed as follows:

$$m_L = \frac{m_H (h_6 - h_1) + m_{jw} c_{pw} (T_{jw1} - T_{jw2})}{(h_{4'} - h_{3'})} \tag{8}$$

$$T_{jw2} = T_{3'} + \Delta T_{pp2} \tag{9}$$

When the PPTD of the preheater occurs at State point 2', the mass flow rate is expressed as follows:

$$m_L = \frac{m_H(h_6 - h_1) + m_{jw}c_{pw}(T_{jw1} - T_{jw3})}{(h_{4'} - h_{2'})} \tag{10}$$

$$T_{jw3} = T_{2'} + \Delta T_{pp2} \tag{11}$$

where c_{pw} is the specific heat capacity of the jacket cooling water at constant pressure, which is set to 4.18 kJ/(kg·K); m_{jw} is the jacket cooling water mass flow rate; T_{jw} is the jacket cooling water temperature; and ΔT_{pp2} is the LTL preheater PPTD.

If $T_{3'} + T_{pp2} > T_{jw1}$, then Case 2 occurs (Figure 3b). The LTL working fluid is only preheated to State point 7'. When the PPTD of the preheater is at State point 7', m_L is calculated as follows:

$$m_L = \frac{m_H(h_6 - h_1)}{(h_{4'} - h_{7'})} \tag{12}$$

$$h_{7'} = f(p_{Le}, T_{7'}) \tag{13}$$

$$T_{7'} = T_{jw1} - \Delta T_{pp2} \tag{14}$$

where p_{Le} is the LTL evaporation pressure.

When the PPTD of the preheater occurs at State point 2', m_L is obtained using Equations (10) and (11).

The cooling water mass flow rate is calculated as follows:

$$m_w = \frac{m_L(h_{6'} - h_{1'})}{c_{pw}(T_{w2} - T_{w1})} \tag{15}$$

where T_w is the cooling water temperature.

The power consumed by a cooling water pump is

$$P_{pw} = \frac{m_w g H}{\eta_{pw}} \tag{16}$$

where H is the cooling water pump head, and g is the gravitational acceleration, which is set to 9.8 m/s².

The power produced by the LTL turbine is calculated as

$$P_L = m_L(h_{4'} - h_{5's})\eta_t = m_L(h_{4'} - h_{5'}) \tag{17}$$

The power consumed by the LTL working fluid pump can be expressed as

$$P_{LP} = \frac{m_L(h_{2's} - h_{1'})}{\eta_p} = m_L(h_{2'} - h_{1'}) \tag{18}$$

The LTL net power output is

$$P_{Lnet} = P_L - P_{LP} - P_{pw} \tag{19}$$

2.3. System

The system net power output is equal to the HTL net power output plus the LTL net power output

$$P_{net} = P_{Hnet} + P_{Lnet} \tag{20}$$

The engine exhaust gas waste heat and jacket cooling water heat utilization ratios correspond to the following equations:

$$\eta_g = \frac{T_{g1} - T_{g3}}{T_{g1} - T_0} \tag{21}$$

$$\eta_{jw} = \frac{T_{jw1} - T_{jw3}}{T_{jw1} - T_0} \tag{22}$$

where T_0 is the ambient temperature set to 288.15 K [42].

The thermal efficiency is expressed as follows:

$$\eta_{th} = \frac{P_{net}}{m_g c_{pg}(T_{g1} - T_{g3}) + m_{jw} c_{pw}(T_{jw1} - T_{jw3})} \tag{23}$$

2.4. Exergy

The system exergy efficiency can be obtained using the following equation:

$$\eta_{ex} = \frac{P_{net}}{E_{tot}} \tag{24}$$

where E_{tot} is the total exergy [29,30]:

$$E_{tot} = m_g c_{pg} \left[(T_{g1} - T_0) - T_0 \ln \left(\frac{T_{g1}}{T_0} \right) \right] + m_{jw} c_{pw} \left[(T_{jw1} - T_{jw3}) - T_0 \ln \left(\frac{T_{jw1}}{T_{jw3}} \right) \right] \tag{25}$$

The exergy destruction rate of each component can be calculated as follows:

$$I = \frac{E_d}{E_{tot}} \tag{26}$$

where E_d is the exergy destruction of each component. The calculation formulations are summarized in Table 2.

Table 2. Calculation formulation of exergy destruction.

Components	Exergy Destruction
HTL evaporator	$E_{dHe} = m_g c_{pg} [(T_{g1} - T_{g3}) - T_0 \ln(T_{g1}/T_{g3})] - m_H [(h_5 - h_2) - T_0(s_5 - s_2)]$
condenser/evaporator	$E_{dce} = m_H [(h_6 - h_1) - T_0(s_6 - s_1)] - m_L [(h_{4'} - h_{7'}) - T_0(s_{4'} - s_{7'})]$
HTL turbine	$E_{dHt} = m_H T_0 (s_6 - s_5)$
HTL working fluid pump	$E_{dHp} = m_H T_0 (s_2 - s_1)$
exhaust gas from HTL evaporator	$E_{dHeout} = m_g c_{pg} [(T_{g3} - T_0) - T_0 \ln(T_{g3}/T_0)]$
LTL preheater	$E_{dLpre} = m_{jw} c_{pw} \left[(T_{jw1} - T_{jw3}) - T_0 \ln \left(\frac{T_{jw1}}{T_{jw3}} \right) \right] - m_L [(h_{7'} - h_{2'}) - T_0(s_{7'} - s_{2'})]$
LTL condenser	$E_{dLc} = m_L [(h_{5'} - h_{1'}) - T_0(s_{5'} - s_{1'})]$
LTL turbine	$E_{dLt} = m_L T_0 (s_{5'} - s_{4'})$
LTL working fluid pump	$E_{dLp} = m_L T_0 (s_{2'} - s_{1'})$

2.5. Assumptions

The following assumptions are created to simplify the analysis:

- (1) The DORC system is in a steady state.
- (2) The pump and turbine efficiencies are constant.
- (3) The heat losses and pressure drops are neglected.

3. Model Validation

The model in the present work is consistent with the author’s previous article [43] and is compared with DORC data of Literature [29,30]; Table 3 displays the comparison results. The HTL net power outputs in the present work are consistent with the literature, and the maximal relative error is 2.1%. Moreover, the calculation accuracy is reliable.

Table 3. Data comparison between the present work and the literature.

	HTL	LTL	HTL	LTL
	Cyclohexane	R245fa	Toluene	R236fa
evaporation temperature/K	480.3	349.0	440.3	378.9
net power output/kW (literature [29])	64.0	47.2	32.6	64.6
net power output/kW (present work)	64.01	46.58	32.61	63.59
relative error/%	0.0	1.3	0.0	1.6

	HTL	LTL		
	Water	R123	R236fa	R245fa
evaporation temperature/K	480.0	347.5	369.0	352.3
net power output/kW (literature [30])	54.5	46.0	60.6	49.4
net power output/kW (present work)	54.52	45.21	59.32	48.53
relative error/%	0.0	1.7	2.1	1.8

$$\text{Relative error} = | \text{data of present work} - \text{data of literatures} | / \text{data of literatures} \times 100\%$$

4. Optimization Method

The net power output is the objective function. Optimization variables include HTL evaporation temperature (T_3), HTL condensation temperature (T_1), and HTL superheat degree ($T_5 - T_4$). The optimization ranges are listed in Table 4. The lower limit of T_3 is T_1 plus 5 K. The difference between working fluid critical temperature and the upper limit of T_3 must be 15 K to prevent the HTL working fluid from approaching the critical point. The lower limit of T_1 is HTL working fluid saturated temperature at the pressure of 101 kPa to avoid the contamination of non-condensable gases [29,30,43]; the upper limit is the LTL working fluid critical temperature minus 15 K and then plus ΔT_{pp2} to avoid the LTL working fluid from approaching the critical point. The lower limit of HTL superheat degree is 0 K, and the upper limit is T_{g1} minus ΔT_{pp1} and T_4 to avoid the heat transfer temperature of the HTL evaporator from being lower than ΔT_{pp1} . In addition, the exhaust gas temperature at the exit of the HTL evaporator must be higher than the acid dew point temperature, which is 373.15 K [42]. By contrast, the LTL evaporation temperature must be lower than the LTL working fluid critical temperature minus 15 K.

Table 4. Optimization ranges of the operating parameters.

Optimization Parameters	Lower Limit	Upper Limit
HTL evaporation temperature	HTL condensation temperature + 5 K	HTL working fluid critical temperature - 15K
HTL condensation temperature	HTL working fluid normal boiling point	LTL working fluid critical temperature - 15K + ΔT_{pp2}
HTL superheat degree	0 K	$T_{g1} - \Delta T_{pp1} - T_4$

The genetic algorithm is a random search method based on the evolution rule of organisms; this algorithm was invented by Prof. Holland in 1975 on the basis of the ideas of natural selection. The genetic algorithm mainly includes selection, crossover, and mutation calculations. Selection calculation selects good individuals from the generation. Crossover calculation is used for individuals to generate new individuals. Mutation calculation is adopted to avoid a local optimal solution. In the genetic algorithm, a population of candidate solutions to an optimization problem is evolved toward improved solutions. When the genetic algorithm is used, a population of randomly generated individuals is selected as the initial population, and iterative calculation begins. The population in each iteration is called a generation. The fitness of every individual in the population is calculated in each generation. If it does not satisfy the stopping criteria, then the more fit individuals are randomly selected from the population, and each individual is modified by crossover and mutation operators for creating a new generation. The new generation of candidate solutions is used for net iteration. When an appropriate fitness level is reached or the maximal generations are formed, the calculation is

terminated, and the results are shown [6,44]. A flowchart of the genetic algorithm is demonstrated in Figure 4.

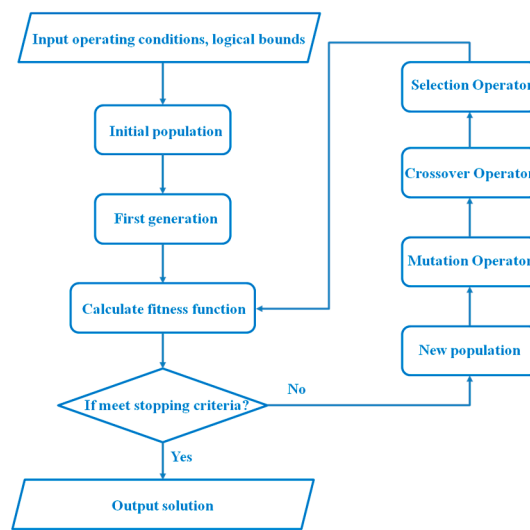


Figure 4. Flowchart of the genetic algorithm.

The genetic algorithm has been extensively used for optimization [6,37,45–51]. Yang et al. [6] selected a net power output per unit heat transfer area and exergy destruction rate as the objective functions and optimized evaporation pressure, superheat degree, and condensation temperature for ORC using the genetic algorithm. Xi et al. [46] set exergy efficiency as the objective function and performed turbine inlet pressure, turbine inlet temperature, and the fractions of the flow rate of the regenerative optimization for an ORC through the genetic algorithm. Wang et al. [47] selected a ratio of the net power output to the total heat transfer area as the performance evaluation criterion and optimized key thermodynamic design parameters for the ORC through the genetic algorithm. Thus, the present work used the genetic algorithm in MATLAB for optimization, and the parameter setting of the genetic algorithm is presented in Table 5. The fluid properties are calculated using Refprop 9.0.

Table 5. Parameter setting of the genetic algorithm.

Parameters	Value
population size	50
crossover fraction	0.8
maximal generations	500
function tolerance	10 ^{−6}

5. Result and Discussion

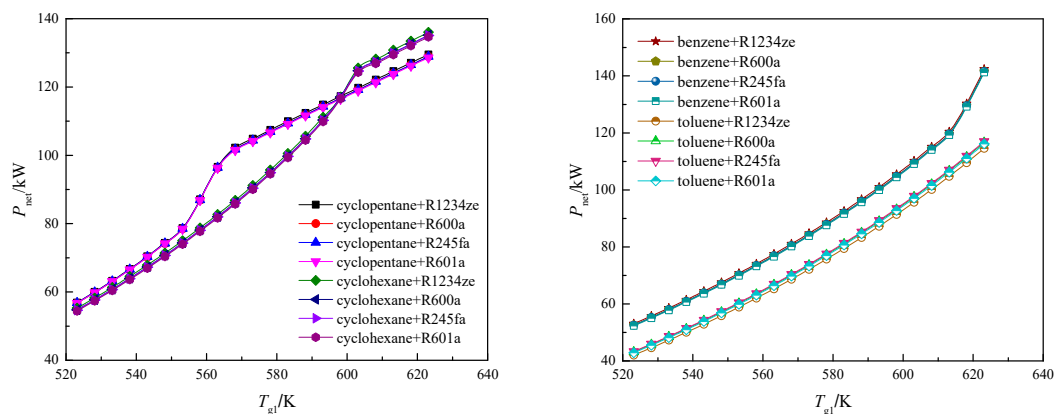
The data of ICE are from an inline six-cylinder turbocharged engine. The exhaust gas mass flow rate is 7139 kg/h; the jacket cooling water mass flow rate and temperature are 6876 kg/h and 363.15 K, correspondingly [18]. The PPTD of the HTL evaporator is the largest [5,19] because the heat transfer performance of engine exhaust gas is low; the PPTD of the HTL evaporator is set to 20 K on the basis of Literature [18,43]; the PPTDs of the LTL preheater and condenser/evaporator are set to 10 K on the basis of Literature [40,43]; and PPTD of 5 K is common for an LTL condenser [5,19,40,43]. The DORC parameters are listed in Table 6 [43].

Table 6. DORC parameters.

Parameters	Symbol	Value
PPTD of HTL/K	ΔT_{pp1}	20
PPTD of LTL preheater and condenser/evaporator/K	ΔT_{pp2}	10
PPTD of LTL condenser/K	ΔT_{pp3}	5
cooling water inlet temperature/K	T_{w1}	298.15
cooling water outlet temperature/K	T_{w3}	303.15
turbine efficiency/%	η_t	80
working fluid pump efficiency/%	η_p	75
cooling water pump efficiency/%	η_{pw}	85
cooling water pump head/m	H	20
ambient temperature/K	T_0	288.15

5.1. Thermal Performance

In Figure 5, the net power output increases with T_{g1} . The DORC net power output is mainly affected by HTL working fluids, and LTL working fluids have minimal influence on the net power output. When HTL working fluids are the same, the relative deviation ($| \text{maximal net power output} - \text{minimal net power output} | / \text{minimal net power output} \times 100\%$) of the net output power affected by different LTL working fluids is less than 3%. Thus, selecting a suitable HTL working fluid is important. When T_{g1} is 523.15–598.15 K, cyclopentane and R1234ze(E) are used, and the maximal net power output is 56.9–117.3 kW. When T_{g1} is 603.15–618.15 K, cyclohexane and R1234ze(E) are used, and the maximal net power output is 125.6–133.4 kW. When T_{g1} is raised to 623.15 K, the HTL and LTL optimal working fluids are benzene and R1234ze(E), respectively, and the maximal net power output is 142.4 kW. Table 7 presents the optimal working fluids and the corresponding net power outputs. R1234ze(E) is optimal for LTLs when the HTL working fluids are cyclopentane, cyclohexane, and benzene. T_{g1} will not affect the optimal LTL working fluid. When the HTL working fluid is toluene, the PPTD of the condenser/evaporator will be higher than ΔT_{pp2} when R1234ze(E) is used for the LTL considering the lower limits of the HTL condensation and the LTL evaporation temperatures. Therefore, R245fa is used for maximizing the net power output.



(a) Cyclopentane and cyclohexane are used for HTL. (b) Benzene and toluene are used for HTL.

Figure 5. Effects of T_{g1} on the net power output.

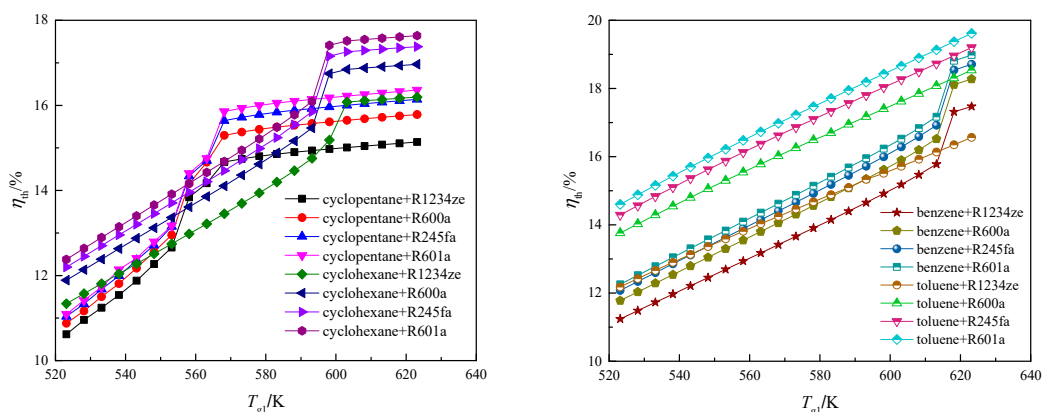
Table 7. Optimal working fluids and net power output with T_{g1} of 523.15–623.15 K.

T_{g1}/K	HTL Working Fluid	LTL Working Fluid	Maximal Net Power Output/kW
523.15–598.15	cyclopentane	R1234ze(E)	56.9–117.3
603.15–618.15	cyclohexane	R1234ze(E)	125.6–133.4
623.15	benzene	R1234ze(E)	142.4

In Figure 5a, when cyclopentane is used for HTL, the net power output increases with T_{g1} . The optimal HTL evaporation temperature does not reach the upper limit when T_{g1} is 523.15–553.15 K, and the increasing trend of the net power output remains unchanged. The optimal HTL evaporation temperature reaches the upper limit, and the optimal HTL superheat degree is 0 K when T_{g1} increases to 558.15 K. The HTL evaporation temperature is suitable for T_{g1} , and the increment rate of the net power output increases. The evaporation temperature becomes unsuitable for increasing T_{g1} , and the optimal HTL superheat degree is not 0 K when T_{g1} increases to 568.15 K. The increment rate of the net power output decreases. When cyclohexane is used for the HTL, T_{g1} is 523.15–598.15 K, the optimal HTL evaporation temperature does not reach the upper limit, and the PPTD of the HTL evaporator is at VPP. The net power output increases with the T_{g1} . When T_{g1} increases to 603.15 K, the PPTD of the HTL evaporator occurs at PPP, T_{g3} cannot decrease, and the increment rate of net power output decreases.

Figure 5b exhibits that, when benzene is used for HTL and T_{g1} is 523.15–613.15 K, the optimal HTL evaporation temperature does not reach the upper limit, and the net power output increases with T_{g1} . The optimal HTL evaporation temperature reaches the upper limit, and the PPTD of the HTL evaporator is at VPP when T_{g1} rises to 618.15 K. Furthermore, T_{g3} rapidly decreases with the increase in T_{g1} , thereby increasing the increment rate of the net power output. The optimal HTL evaporation temperature does not reach the upper limit, and the PPTD of the HTL evaporator occurs at VPP when toluene is used for the HTL, and T_{g1} is 523.15–623.15 K. Therefore, the net power output increases with T_{g1} .

Figure 6 illustrates that thermal efficiency increases with T_{g1} because the increment rate is larger in the net power output than in heat absorption. The maximal thermal efficiency is 14.6–19.6% with the T_{g1} of 523.15–623.15 K when toluene and R601a are used for HTL and LTL, correspondingly. The thermal efficiencies of cyclopentane, cyclohexane, and benzene system are also maximal when R601a is used for LTL. The R1234ze(E) used for the LTL will cause minimal thermal efficiency.



(a) Cyclopentane and cyclohexane are used for HTL. (b) Benzene and toluene are used for HTL.

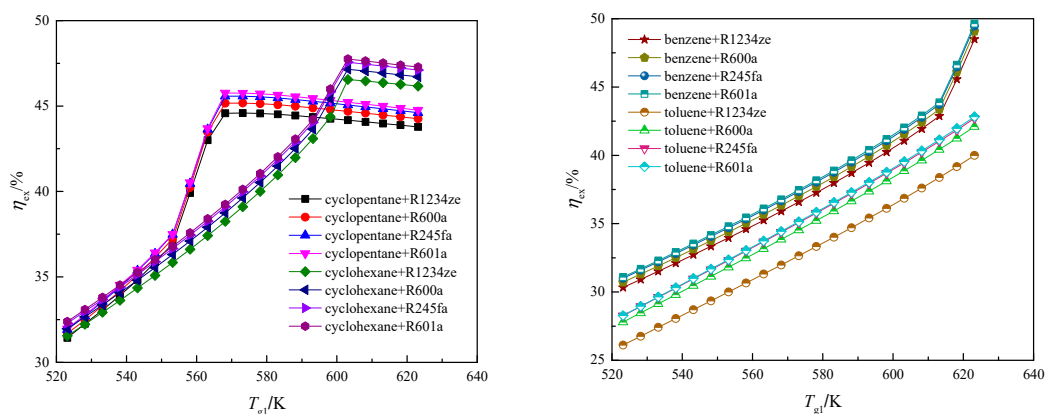
Figure 6. Effects of T_{g1} on the thermal efficiency.

Figure 6a shows that the optimal HTL evaporation temperature does not reach the upper limit when cyclopentane is used for HTL, and T_{g1} is 523.15–553.15 K. The thermal efficiency increases with T_{g1} . The net power output increases rapidly when T_{g1} is 558.15–563.15 K, thus also rapidly

increasing thermal efficiency. The HTL evaporation temperature is unsuitable for the increase in T_{g1} , the increment rates of the net power output and thermal efficiency decrease when T_{g1} increases to 568.15 K. When cyclohexane is used and T_{g1} is 523.15–593.15 K, the optimal HTL evaporation temperature does not reach the upper limit, and the thermal efficiency increases with T_{g1} . When T_{g1} increases to 598.15 K, the optimal HTL evaporation temperatures of the R600a, R245fa, and R601a systems reach the upper limit; moreover, the irreversibilities between exhaust gas and HTL increase, and the increment rate of thermal efficiency decreases. For the R1234ze(E) system, the optimal HTL evaporation temperature reaches the upper limit with the T_{g1} of 603.15 K.

Figure 6b demonstrates that, when benzene is used for HTL, and T_{g1} is 523.15–613.15 K, the optimal HTL evaporation temperature does not reach the upper limit, and the thermal efficiency increases with T_{g1} . When T_{g1} increases to 618.15 K, the optimal HTL evaporation temperature reaches the upper limit, and the increment rate of thermal efficiency decreases. When toluene is used for HTL, and T_{g1} is 523.15–623.15 K, the optimal HTL evaporation temperature does not reach the upper limit, and the increment rate of thermal efficiency remains unchanged.

Figure 7 displays that the variations in exergy efficiency with T_{g1} are different with various HTL working fluids. Furthermore, Figure 7a illustrates that, when cyclopentane is used for HTL, and T_{g1} is 523.15–553.15 K, the optimal HTL evaporation temperature does not reach the upper limit, the increasing T_{g1} improves net power output, and the exergy efficiency increases with increasing T_{g1} . When T_{g1} is 558.15–563.15 K, the optimal HTL evaporation temperature reaches the upper limit, and the optimal HTL superheat degree is 0 K; furthermore, the HTL evaporation temperature is suitable for T_{g1} , and the exergy efficiency increases rapidly with T_{g1} . When T_{g1} increases to 568.15 K, the HTL evaporation temperature is unsuitable for increasing T_{g1} , and the optimal HTL superheat degree is not 0 K; with the increase in T_{g1} , the irreversibilities between exhaust gas and HTL increase, and the exergy efficiency decreases slowly. When cyclohexane is used for HTL, and T_{g1} is 523.15–598.15 K, the optimal HTL evaporation temperature does not reach the upper limit, and the PPTD of the HTL evaporator occurs at VPP; in addition, the exergy efficiency increases with T_{g1} . When T_{g1} increases to 603.15 K, the PPTD of the HTL evaporator occurs at PPP, and the optimal HTL evaporation temperature reaches the upper limit; moreover, T_{g3} cannot decrease, although the increase in T_{g1} will improve the net power output and will increase the irreversibilities between exhaust gas and the HTL given the HTL evaporation temperature upper limit, and the exergy efficiency begins to decrease slowly.



(a) Cyclopentane and cyclohexane are used for HTL. (b) Benzene and toluene are used for HTL.

Figure 7. Effects of T_{g1} on the exergy efficiency.

Figure 7b depicts that, when benzene is used for HTL, and T_{g1} is 523.15–613.15 K, the optimal HTL evaporation temperature does not reach the upper limit, and the exergy efficiency increases with T_{g1} . When T_{g1} increases to 618.15 K, the optimal HTL evaporation temperature reaches the upper limit, and the PPTD of the HTL evaporator occurs at VPP. The HTL evaporation temperature is suitable for T_{g1} at the moment; with the increase in T_{g1} , T_{g3} rapidly decreases, the increment rate of net power

output increases, and then increment rate of exergy efficiency increases. When toluene is used for the HTL, and T_{g1} is 523.15–623.15 K, the optimal HTL evaporation temperature does not reach the upper limit, and the PPTD of the HTL evaporator occurs at VPP; furthermore, with the increase in T_{g1} , the exergy efficiency increases, but the increasing trend is unchanged; when R1234ze(E) is used for LTL, the exergy efficiency is much smaller than that of other systems because the PPTD is higher in the condenser/evaporator than in ΔT_{pp2} . When R601a is used for LTL, the exergy efficiency is maximal; when R1234ze(E) is used for LTL, the exergy efficiency is minimal.

5.2. Operating Parameter

When the HTL working fluid is given, the variation in optimized HTL evaporation temperature, HTL condensation temperature, HTL superheat degree, exhaust gas temperature at the exit of the HTL evaporator and heat utilization ratio, exergy destruction rate with an increase in T_{g1} for the four LTL working fluids are similar, and the systems with maximal net power output for four HTL working fluids are investigated. The four systems identified are cyclopentane + R1234ze(E), cyclohexane + R1234ze(E), benzene + R1234ze(E), and toluene + R245fa.

Figure 8 depicts the effects of T_{g1} on the optimal HTL evaporation temperature. With the increase in T_{g1} , the increasing HTL evaporation temperature can improve temperature match with exhaust gas. The optimal HTL evaporation temperature increases initially for the cyclopentane system. When T_{g1} rises to 558.15 K, the optimal HTL evaporation temperature reaches the upper limit. When cyclohexane is used for HTL, the optimal HTL evaporation temperature increases initially with T_{g1} . When T_{g1} rises to 603.15 K, the optimal HTL evaporation temperature reaches the upper limit. When benzene is used for HTL, the optimal HTL evaporation temperature initially increases with T_{g1} . When T_{g1} rises to 618.15 K, the optimal HTL evaporation temperature reaches the upper limit. Given the high upper limit of the HTL evaporation temperature, for the toluene system, the optimal HTL evaporation temperature increases with T_{g1} .

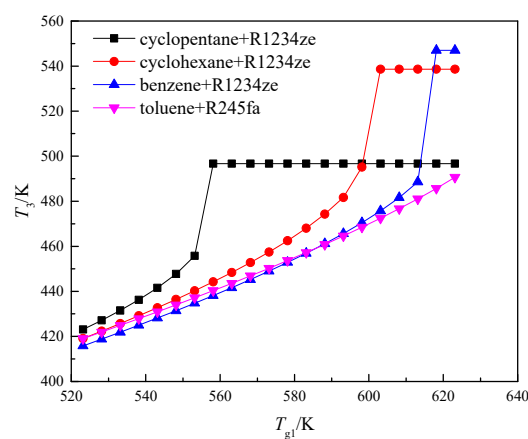


Figure 8. Effects of T_{g1} on the optimal HTL evaporation temperature.

Figure 9 demonstrates the effects of the T_{g1} on the optimal HTL condensation temperature. The optimal HTL condensation temperature remains unchanged for cyclohexane, benzene, and toluene systems, and the optimal HTL condensation temperature is the lower limit (the saturated temperature at the pressure of 101 kPa); moreover, the low HTL condensation temperature will enhance the DORC performance, and similar results are obtained by several parameter analysis studies [5,21,23,43]. The optimal HTL condensation temperature increases with 523.15–563.15 K T_{g1} when cyclopentane is used for HTL, and the saturated cycle is used. The superheated cycle is used when T_{g1} is raised to 568.15 K, and the optimal HTL condensation temperature remains unchanged. It is higher than the lower limit (322.3 K) because the decrease in HTL condensation temperature will decrease T_{g3} , and T_{g3} must be higher than or equal to the exhaust gas acid dew point temperature to

avoid low-temperature acid corrosion. Moreover, when the HTL condensation temperature increases to 351.0 K, T_{g3} is equal to the exhaust gas acid dew point temperature and maintains at 351.0 K.

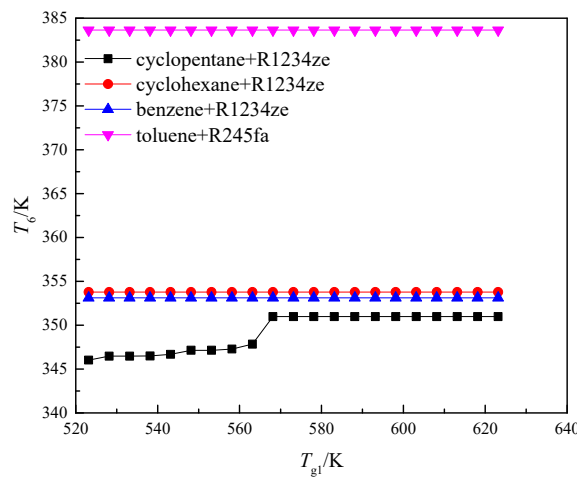


Figure 9. Effects of T_{g1} on the optimal HTL condensation temperature.

The HTL evaporation temperature upper limits are high, given the high critical temperatures of cyclohexane, benzene, and toluene. When T_{g1} increases, the increasing HTL evaporation temperature can improve the temperature match with the heat source, the superheated cycle is unnecessary, and the optimal HTL superheat degree is 0 K for cyclohexane, benzene, and toluene systems. In particular, the saturated cycle will generate more power output than the superheated cycle for these systems. However, the HTL evaporation temperature upper limit for the cyclopentane system is lower than other working fluids. When T_{g1} increases to 568.15 K, the HTL evaporation temperature is unsuitable for increasing T_{g1} , and the superheated cycle is used to improve temperature match between the engine exhaust gas and HTL given the limit of the HTL evaporation temperature. In Figure 10, when T_{g1} is 523.15–563.15 K, the saturated cycle is improved; when T_{g1} is 568.15–623.15 K, superheated cycle will increase the net power output, the optimal HTL superheat degree increases initially with the increase in T_{g1} and then remains unchanged upon reaching 16.3 K (16.3 K is not the upper limit of optimization setting), and the maximum optimal superheat degree is independent of T_{g1} .

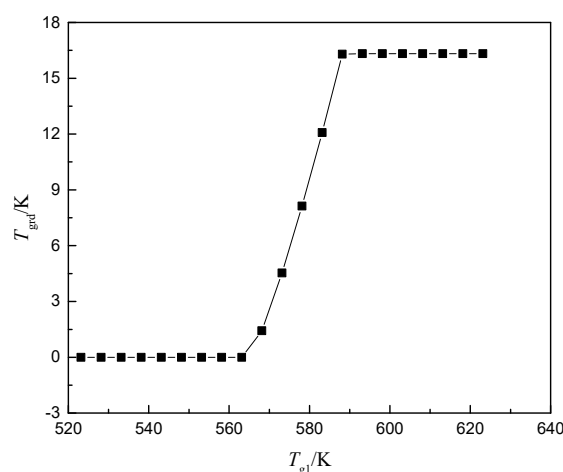


Figure 10. Effects of T_{g1} on the optimal HTL superheat degree for the cyclopentane system.

5.3. Exhaust Gas Temperature at the Exit of the HTL Evaporator and Heat Utilization Ratio

In Figure 11, the variation trend in T_{g3} with T_{g1} is different with varying HTL working fluid systems. T_{g3} of the cyclopentane system decreases with T_{g1} of 523.15–553.15 K, and the optimal HTL

evaporation temperature is not the upper limit. T_{g3} decreases with the increase in T_{g1} . When T_{g1} rises to 558.15 K, the optimal HTL evaporation temperature reaches the upper limit, and T_{g3} increases and then decreases. When T_{g1} rises to 568.15 K, the superheated cycle is used, and T_{g3} reaches the lower limit. Initially, when cyclohexane is used, T_{g3} decreases with the increase in T_{g1} . When T_{g1} increases to 603.15 K, the PPTD of the HTL evaporator occurs at PPP, T_{g3} increases, and then remains at 375.5 K. T_{g3} of the benzene system increases initially and then decreases with the T_{g1} of 523.15–613.15 K. When the T_{g1} increases to 618.15 K, the optimal HTL evaporation temperature reaches the upper limit, and T_{g3} increases and then decreases rapidly with the increase in T_{g1} . Considering that the lower limit of the HTL condensation temperature for the toluene system is the highest, the optimal HTL condensation temperature of this system is higher than the other systems, and T_{g3} of the toluene system is higher than the other systems. With the increase in T_{g1} , T_{g3} increases initially and later decreases. When the net power output is maximal, T_{g3} is not constantly at the lower limit and will be affected by a cycle type (saturated or superheated cycle), the HTL evaporator temperature value, and the PPTD of an HTL evaporator.

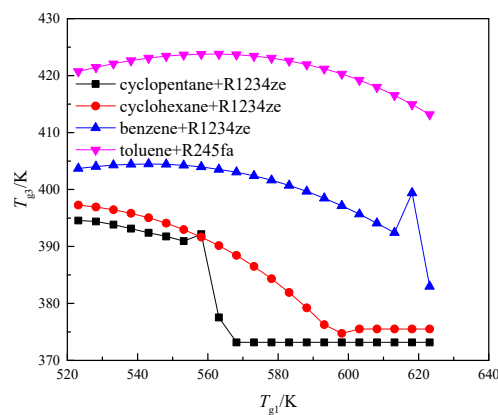


Figure 11. Effects of T_{g1} on the exhaust gas temperature at the exit of the HTL evaporator.

Figure 12 illustrates the variation trend of η_g with T_{g1} . When cyclopentane is used for HTL, and T_{g1} is 523.15–553.15 K, the optimal HTL evaporation temperature does not reach the upper limit, and the increase in T_{g1} decreases T_{g3} . With the increase in T_{g1} , η_g increases. When T_{g1} is 558.15–563.15 K, the optimal HTL evaporation temperature reaches the upper limit, and the optimal HTL superheat degree is 0 K. With the increase in T_{g1} , T_{g3} initially increases and later rapidly decreases; although T_{g3} initially increases with small degrees, T_{g1} increases. With the increase in T_{g1} , η_g increases slowly and later rapidly increases. When T_{g1} increases to 568.15 K, the superheated cycle is used, and T_{g3} remains unchanged. In Equation (21), η_g increases. When cyclohexane is used for HTL, and T_{g1} is 523.15–598.15 K, the optimal HTL evaporation temperature does not reach the upper limit, and the PPTD of HTL evaporator occurs at VPP. η_g increases with the increase in T_{g1} . When T_{g1} increases to 603.15 K, the PPTD of HTL evaporator occurs at PPP, and the optimal HTL evaporation temperature reaches the upper limit, T_{g3} cannot decrease, and the increment rate of η_g decreases. When benzene is used for HTL, and T_{g1} is 523.15–613.15 K, the optimal HTL evaporation temperature does not reach the upper limit. η_g increases with the increase in T_{g1} . When T_{g1} is 618.15–623.15 K, the optimal HTL evaporation temperature reaches the upper limit, and the PPTD of the HTL evaporator remains at State point three. T_{g3} increases initially and then decreases rapidly, and η_g decreases initially and then increases rapidly. When toluene is used for HTL, and T_{g1} is 523.15–623.15 K, the optimal HTL evaporation temperature does not reach the upper limit. With the increase in T_{g1} , η_g is mainly affected by the increase in T_{g1} , although T_{g3} increases initially and later decreases, while η_g increases. When cyclopentane is used for HTL, and T_{g1} is 623.15 K, the maximal η_g is 74.6%.

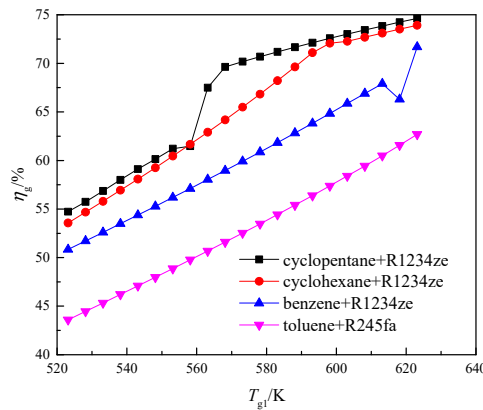


Figure 12. Effects of T_{g1} on the heat utilization ratio of the engine exhaust gas.

In Figure 13, with the increase in T_{g1} , η_{jw} of the cyclopentane system increases initially, then decreases, and finally increases. When T_{g1} increases from 563.15 K to 568.15 K, the cycle type changes from saturated to superheated. η_{jw} decreases with the increase in T_{g1} . With the increase in T_{g1} , η_{jw} increases for the cyclohexane and toluene systems. η_{jw} of the benzene system increases initially with the increase in T_{g1} . When T_{g1} increases to 618.15 K, the optimal HTL evaporation temperature reaches the upper limit and the PPTD of the HTL evaporator still occurs at VPP, and η_{jw} decreases initially and later increases. Considering that the optimal HTL condensation temperatures of the cyclopentane, cyclohexane, and toluene systems are lower than T_{jw1} , Case 1 occurs, and η_{jw} is higher than 35%. When toluene is used, Case 2 occurs, η_{jw} is lower than 26%, and Case 2 must be avoided. The cyclopentane system has a higher η_{jw} than the other systems. When T_{g1} is 623.15 K, the maximal η_{jw} is 51.8%. An increase in T_{g1} can improve η_{jw} .

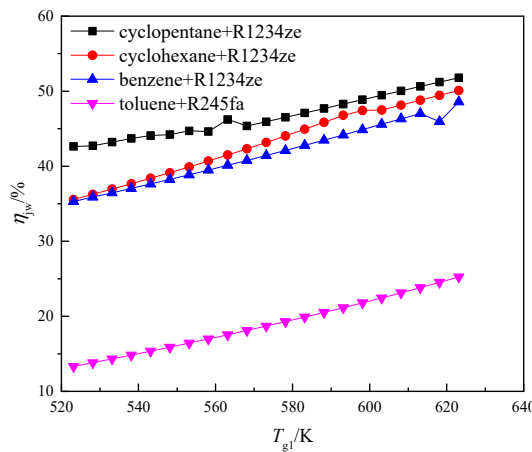


Figure 13. Effects of T_{g1} on the heat utilization ratio of the jacket cooling water.

5.4. Exergy Destruction Rate

The reduction in system exergy destruction is an effective means of improving the system net output power. The investigation of exergy destruction can identify the component with the most potential for reducing exergy destruction. The present work focuses on the exergy destruction rates of exhaust gas from HTL evaporator (I_{Hout}), LTL condenser (I_{Lc}), HTL evaporator (I_{He}), condenser/evaporator (I_{ce}), LTL preheater (I_{Lpre}), HTL turbine (I_{Ht}), LTL turbine (I_{Lt}), and working fluid pumps (I_p) with T_{g1} for different HTL working fluids.

Figure 14 illustrates that, when cyclopentane is used for HTL, I_{Hout} and I_{Lpre} decrease with the increase of T_{g1} , because η_g and η_{jw} are improved by increasing T_{g1} . Because the superheat degree is 0 K and the optimal HTL evaporation temperature initially fails to reach the upper limit, then reaches

the upper limit, and superheat degree is finally not 0 K. I_{Lc} initially declines and then increases with T_{g1} . I_{He} decreases initially with the increase in T_{g1} because the HTL evaporation temperature can increase with the increase in T_{g1} to improve temperature match. Afterward, the superheated cycle is used given the upper limit of the HTL evaporation temperature, which is unsuitable for increasing T_{g1} , thereby increasing I_{He} . I_{He} decreases initially and then increases with T_{g1} . Moreover, I_{ce} , I_{Ht} , and I_p increase initially and then decrease eventually. The variation in I_{Lt} is also affected by the HTL evaporation temperature and superheat degree. I_{Lt} remains unchanged initially, later increases, and finally decreases slowly with the increase in T_{g1} . When T_{g1} is 523.15–538.15 K, I_{out} is maximal at higher than 17% because η_g is low. Furthermore, I_{Lc} is the second largest exergy destruction rate. When T_{g1} is 543.15–623.15 K, the η_g is improved by increasing T_{g1} , and I_{Lc} is maximal at higher than 15.5%. When T_{g1} is 543.15–608.15 K, I_{Hout} is the second largest exergy destruction rate at less than 10%; when T_{g1} is 613.15–623.15 K, I_{He} increases and becomes the second largest given the upper limit of the HTL evaporation temperature. The condenser/evaporator is also a component, which has a large exergy destruction rate. When T_{g1} is 578.15–593.15 K, I_{ce} exceeds I_{He} and becomes the third largest exergy destruction rate. When T_{g1} is 523.15–553.15 K, I_{Lpre} is the fourth largest exergy destruction rate at higher than 5%; when T_{g1} is 573.15–623.15 K, the heat absorption ratio of the jacket cooling water accounting for the total heat absorption decreases, and I_{Lpre} decreases and becomes the second smallest exergy destruction rate considering the increase in exhaust gas heat absorption. When T_{g1} is 568.15 K, the variation in I_{Ht} is larger than I_{Lt} because the HTL cycle type changes from a saturated to a superheated cycle. I_p is minimal at less than 1%.

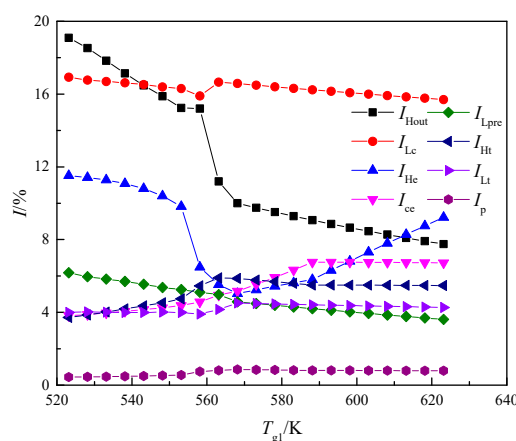


Figure 14. Effects of T_{g1} on exergy destruction rate for the cyclopentane system.

Figure 15 presents that, when cyclohexane is used for HTL, I_{Hout} and I_{Lpre} decrease with the increase in T_{g1} because η_g and η_{jw} are improved by increasing T_{g1} . When T_{g1} is 523.15–598.15 K, the optimal HTL evaporation temperature does not reach the upper limit and is suitable for T_{g1} . I_{He} decreases initially; when T_{g1} increases to 603.15 K, the optimal HTL evaporation temperature reaches the upper limit and is unsuitable for T_{g1} . I_{He} then increases. Given that the optimal HTL evaporation temperature does not reach the upper limit initially, the variation in I_{Lc} is small. With the increase in T_{g1} , I_{Lc} initially decreases and later increases; given the increase in I_{He} , I_{Lc} decreases with the increase in T_{g1} when the optimal HTL evaporation temperature reaches the upper limit. An unchanged HTL condensation temperature corresponds to a small variation in I_{Lt} . I_{Lt} initially decreases, then increases, and finally decreases with the increase in T_{g1} . Considering that I_{He} decreases initially and then increases, I_{ce} , I_{Ht} , and I_p increase initially and later decrease with the increase in T_{g1} . When T_{g1} is 523.15–553.15 K, I_{out} is maximal at higher than 16%, and I_{Lc} is the second largest exergy destruction rate. When T_{g1} is 558.15–623.15 K, I_{out} decreases from 15.3% to 8.2% and becomes the second largest exergy destruction rate given the improvement of η_g by increasing T_{g1} ; I_{Lc} is maximal at higher than 15%. When T_{g1} is 523.15–598.15 K, I_{He} is the third largest exergy destruction rate. However, when T_{g1}

increases to 603.15 K, I_{He} rapidly decreases to 4.1% and becomes the sixth largest exergy destruction rate. When T_{g1} is 603.15–623.15 K, I_{ce} is the third largest exergy destruction rate at higher than 7.5%. When T_{g1} is 523.15–553.15 K, I_{Lpre} is the fourth largest exergy destruction rate at higher than 5%; when T_{g1} is 573.15–623.15 K, I_{Lpre} becomes the second smallest exergy destruction rate. Given the increasing heat absorption from exhaust gas with increasing T_{g1} , I_{Ht} is higher than I_{Lt} when T_{g1} is 583.15–623.15 K. Considering that the optimal HTL condensation temperature is constant, a minimal change in I_{Lt} is observed. I_p is the smallest exergy destruction rates of the system.

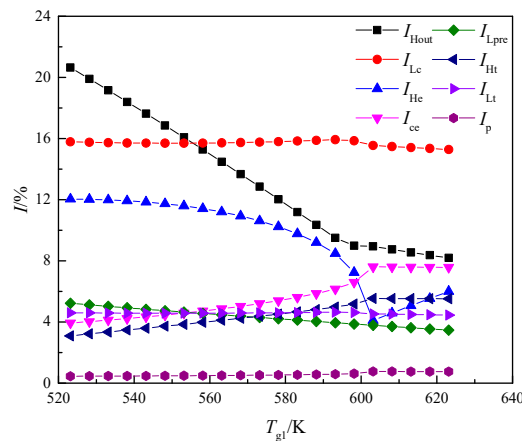


Figure 15. Effects of T_{g1} on exergy destruction rate for the cyclohexane system.

Figure 16 exhibits that the optimal HTL evaporation temperature does not reach the upper limit when T_{g1} is 523.15–613.15 K because benzene is used for HTL. Thus, η_g is improved by increasing T_{g1} , and I_{Hout} decreases with the increase in T_{g1} . When T_{g1} increases to 618.15 K, the optimal HTL evaporation temperature reaches the upper limit, and η_g decreases and then I_{Hout} increases; when T_{g1} increases to 623.15 K, I_{Hout} later decreases considering the increase in η_g . Given the increase in η_{jw} , I_{Lpre} decreases with the increase in T_{g1} . Considering that the optimal HTL evaporation temperature does not reach the upper limit, I_{He} increases initially and later decreases with the increase in T_{g1} . The variation is small; when T_{g1} increases to 618.15 K, the optimal HTL evaporation temperature reaches the upper limit, and I_{He} decreases rapidly. The sudden changes in 618.15–623.15 K for other components are also affected by the value of the HTL evaporation temperature. With the increase in T_{g1} , I_{Lc} and I_{Lt} decrease initially and later increase. I_{ce} , I_{Ht} , and I_p increase with T_{g1} . When T_{g1} is 523.15–588.15 K, I_{Hout} is the largest exergy destruction rate at higher than 15%. When T_{g1} is 593.15–623.15 K, I_{Hout} decreases considerably and then I_{Lc} becomes the largest given the improvement of η_g . When T_{g1} is 523.15–613.15 K, I_{He} is the third largest. When T_{g1} is 618.15–623.15 K, I_{He} decreases rapidly to 4.8%, and I_{Ht} becomes the third largest because the optimal HTL evaporation temperature reaches the upper limit. When T_{g1} is 588.15–623.15 K, I_{Lpre} is the second smallest; the I_p is the smallest.

In Figure 17, when toluene is used for HTL no sudden changes are observed because the optimal HTL evaporation temperature does not reach the upper limit. Given the improvement of η_g , I_{Hout} decreases with the increase in T_{g1} . Considering that the optimal HTL evaporation temperature increases with T_{g1} , I_{He} decreases with the increase in T_{g1} . Furthermore, I_{Lc} , I_{ce} , and I_{Ht} increase with T_{g1} due to the decrease in I_{Hout} and I_{He} . Given that the HTL condensation temperature is unchanged and the power consumed by the pump is small, the relative variations in I_{Lpre} , I_{Lt} , and I_p are less than 0.5% between the maximal and minimal values. Considering the low η_g , I_{Hout} is the largest exergy destruction rate, and it is followed by I_{Lc} and I_{He} . I_p , I_{Lpre} , and I_{Ht} are less than the other components with T_{g1} of 523.15–623.15 K.

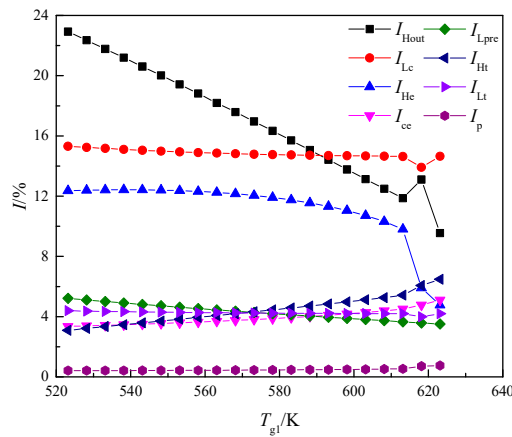


Figure 16. Effects of T_{g1} on exergy destruction rate for the benzene system.

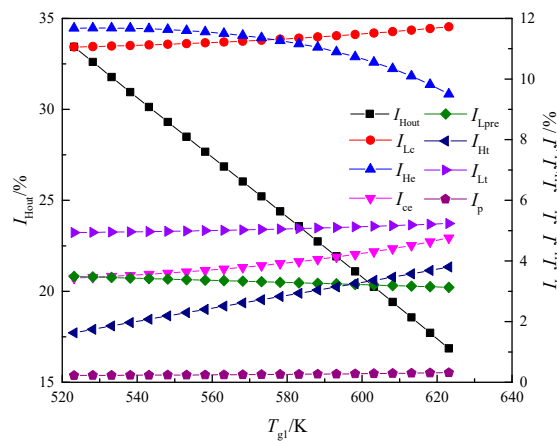


Figure 17. Effects of T_{g1} on exergy destruction rate for the toluene system.

The variations in the exergy destruction rate with T_{g1} are different for various HTL working fluids. I_{Hout} and I_{Lc} are the top two in most cases, but I_{He} and I_{ce} are also important. Given the limit of acid dew point temperature, I_{Hout} is inevitable for the cyclopentane system; an increase in T_{g1} will improve η_g for the cyclohexane, benzene, and toluene systems. Moreover, when cyclopentane is used, and T_{g1} is 623.15 K, I_{Hout} is decreased to 7.8%. Considering the isothermal phase characteristic of pure fluids (When pure working fluid evaporates or condenses at constant pressure, the evaporation or condensation temperature is also constant), significant irreversibilities are observed in the HTL evaporator and LTL condenser [3,52,53], thus leading to large I_{Lc} and I_{He} . The use of zeotropic mixtures with non-isothermal phase change characteristics will cause improved temperature matches between the ICE exhaust gas and HTL, LTL, and cooling water [3,43] and then decrease I_{Lc} and I_{He} . When T_{g1} is high (higher than or equal to 537.15 K for the cyclopentane and cyclohexane systems, 593.15 K for the benzene system, and 598.15 K for the toluene system), I_{Lpre} is the second smallest exergy destruction rate. I_p is the minimal exergy destruction rate.

6. Conclusions

DORC is used for ICE waste heat recovery. The HTL evaporation temperature, condensation temperature and superheat degree are optimized by genetic algorithm, and the net power output is the objective function. The effects of T_{g1} on net power output, thermal efficiency, exergy efficiency, HTL evaporation temperature, HTL condensation temperature, HTL superheat degree, exhaust gas temperature at the exit of the HTL evaporator, heat utilization ratio, and exergy destruction rate are analyzed.

The main conclusions are obtained as follows:

1. The net power output of the DORC is primarily influenced by the HTL working fluid, and the relative deviation between the maximal and minimal net power outputs affected by the LTL working fluid is less than 3%. When T_{g1} is 523.15–598.15 K, cyclopentane is the optimal HTL working fluid for maximizing the net power output; when T_{g1} is 603.15–618.15 K, cyclohexane is the optimal HTL working fluid; when T_{g1} increases to 623.15 K, benzene is the optimal HTL working fluid. R1234ze(E) is the optimal working fluid of LTL.

2. The optimal HTL evaporator temperature increases with T_{g1} until reaching the upper limit. The optimal HTL condensation temperature initially increases and then remains unchanged for the cyclopentane system; in addition, it is maintained at a lower limit of the HTL condensation temperature for the cyclohexane, benzene, and toluene systems. Saturated cycle is suitable for these systems. Superheat cycle can improve the net power output for the cyclopentane system with T_{g1} of 568.15–623.15 K.

3. The optimal exhaust gas temperature at the exit of the HTL evaporator is not constantly at the lower limit, but is at the lower limit for the cyclopentane system at 568.15–623.15 K; the exhaust gas temperature at the exit of the HTL evaporator is higher than the lower limit for the cyclohexane, benzene and toluene systems. The increase in exhaust gas temperature can improve the heat utilization ratio.

4. Variations in the exergy destruction rates with T_{g1} are distinct for the different HTL working fluid systems. I_{Hout} and I_{Lc} are the top two in most cases. When cyclopentane is used and exhaust gas temperature is 623.15 K, and the minimal I_{Hout} is 7.8%. I_p is the minimal exergy destruction rate.

Author Contributions: Conceptualization, Z.G. and Y.D.; methodology, Z.G. and J.L.; software, Z.G.; validation, Z.G. and J.L.; formal analysis, Z.G. and J.L.; investigation, Z.G.; resources, Y.D. and Z.Y.; data curation, Z.G. and J.L.; writing—original draft preparation, Z.G.; writing—review and editing, Z.G., J.L., Y.D. and Z.X.; visualization, Z.G.; supervision, Y.D.; project administration, Y.D. and Z.Y.; funding acquisition, Y.D., Z.Y. and Z.X.

Funding: This research was funded by National Natural Science Foundation of China, grant number 51736005, 51621062 and 11461078.

Acknowledgments: This work was supported by the National Natural Science Foundation of China (Grant Nos. 51736005, 51621062 and 11461078).

Conflicts of Interest: The authors declare no conflict of interest.

Nomenclature

Nomenclature

c_p	specific heat capacity at constant pressure (kJ/(kg·K))
E	exergy (kW)
g	gravitational acceleration (m/s ²)
H	pressure head (m)
I	exergy destruction rate (%)
h	specific enthalpy (kJ/kg)
m	mass flow rate (kg/s)
P	power (kW)
s	specific entropy (kJ/(kg·K))
T	temperature (K)
ΔT	temperature difference (K)
Greek symbols	
η	efficiency

Subscripts

0	ambient temperature
1-6,1'-7'	state points shown in Fig{ XE "Fig" }. 2-3
c	condenser
ce	condenser/evaporator
d	destruction
dew	dew point
e	evaporator
ex	exergy
g	engine exhaust gas
H	high temperature loop
jw	jacket cooling water
L	low temperature loop
net	net
p	pump
pp	pinch point
tot	total
w	water

References

1. Liu, H.D.; Zhang, H.G.; Yang, F.B.; Hou, X.C.; Yu, F.; Song, S.S. Multi-objective optimization of fin-and-tube evaporator for a diesel engine organic Rankine cycle (ORC) combined system using particle swarm optimization algorithm. *Energy Convers. Manag.* **2017**, *151*, 147–157. [[CrossRef](#)]
2. Yang, F.B.; Cho, H.J.; Zhang, H.G.; Zhang, J. Thermo-economic multi-objective optimization of a dual loop organic Rankine cycle (ORC) for CNG engine waste heat recovery. *Appl. Energy* **2017**, *205*, 1100–1118. [[CrossRef](#)]
3. Liu, Q.; Duan, Y.Y.; Yang, Z. Effect of condensation temperature glide on the performance of organic Rankine cycles with zeotropic mixture working fluids. *Appl. Energy* **2014**, *115*, 394–404. [[CrossRef](#)]
4. Horst, T.A.; Tegethoff, W.; Eilts, P.; Koehler, J. Prediction of dynamic Rankine Cycle waste heat recovery performance and fuel saving potential in passenger car applications considering interactions with vehicles' energy management. *Energy Convers. Manag.* **2014**, *78*, 438–451. [[CrossRef](#)]
5. Zhou, Y.D.; Wu, Y.D.; Li, F.; Yu, L.J. Performance analysis of zeotropic mixtures for the dual-loop system combined with internal combustion engine. *Energy Convers. Manag.* **2016**, *118*, 406–414. [[CrossRef](#)]
6. Yang, F.B.; Zhang, H.G.; Bei, C.; Song, S.S.; Wang, E.H. Parametric optimization and performance analysis of ORC (organic Rankine cycle) for diesel engine waste heat recovery with a fin-and-tube evaporator. *Energy* **2015**, *91*, 128–141. [[CrossRef](#)]
7. Dolz, V.; Novella, R.; García, A.; Sanchez, J. HD Diesel engine equipped with a bottoming Rankine cycle as a waste heat recovery system. Part 1: Study and analysis of the waste heat energy. *Appl. Therm. Eng.* **2012**, *36*, 269–278. [[CrossRef](#)]
8. Li, J.; Liu, Q.; Ge, Z.; Duan, Y.Y.; Yang, Z. Thermodynamic performance analyses and optimization of subcritical and transcritical organic Rankine cycles using R1234ze(E) for 100–200 °C heat sources. *Energy Convers. Manag.* **2017**, *149*, 140–154. [[CrossRef](#)]
9. Li, J.; Ge, Z.; Duan, Y.Y.; Yang, Z.; Liu, Q. Parametric optimization and thermodynamic performance comparison of single-pressure and dual-pressure evaporation organic Rankine cycles. *Appl. Energy* **2018**, *217*, 409–421. [[CrossRef](#)]
10. Li, J.; Ge, Z.; Liu, Q.; Duan, Y.Y.; Yang, Z. Thermo-economic performance analyses and comparison of two turbine layouts for organic Rankine cycles with dual-pressure evaporation. *Energy Convers. Manag.* **2018**, *164*, 603–614. [[CrossRef](#)]
11. Li, J.; Ge, Z.; Duan, Y.Y.; Yang, Z. Performance analyses and improvement guidelines for organic Rankine cycles using R600a/R601a mixtures driven by heat sources of 100 °C–200 °C. *Int. J. Energy Res.* **2019**, *43*, 905–920. [[CrossRef](#)]

12. Shu, G.Q.; Li, X.N.; Tian, H.; Liang, X.Y.; Wei, H.Q.; Wang, X. Alkanes as working fluids for high-temperature exhaust heat recovery of diesel engine using organic Rankine cycle. *Appl. Energy* **2014**, *119*, 204–217. [[CrossRef](#)]
13. Vaja, I.; Gambarotta, A. Internal combustion engine (ICE) bottoming with organic Rankine cycles (ORCs). *Energy* **2010**, *35*, 1084–1093. [[CrossRef](#)]
14. Srinivasan, K.K.; Mago, P.J.; Krishnan, S.R. Analysis of exhaust waste heat recovery from a dual fuel low temperature combustion engine using an Organic Rankine Cycle. *Energy* **2010**, *35*, 2387–2399. [[CrossRef](#)]
15. Hountalas, D.T.; Mavropoulos, G.C.; Katsanos, C.; Knecht, W. Improvement of bottoming cycle efficiency and heat rejection for HD truck applications by utilization of EGR and CAC heat. *Energy Convers. Manag.* **2012**, *53*, 19–32. [[CrossRef](#)]
16. Yu, G.P.; Shu, G.Q.; Tian, H.; Wei, H.Q.; Liu, L.N. Simulation and thermodynamic analysis of a bottoming Organic Rankine Cycle (ORC) of diesel engine (DE). *Energy* **2013**, *51*, 281–290. [[CrossRef](#)]
17. Song, J.; Song, Y.; Gu, C.W. Thermodynamic analysis and performance optimization of an Organic Rankine Cycle (ORC) waste heat recovery system for marine diesel engines. *Energy* **2015**, *82*, 976–985. [[CrossRef](#)]
18. Song, J.; Gu, C.W. Analysis of ORC (Organic Rankine Cycle) systems with pure hydrocarbons and mixtures of hydrocarbon and retardant for engine waste heat recovery. *Appl. Therm. Eng.* **2015**, *89*, 693–702. [[CrossRef](#)]
19. Tian, H.; Liu, L.N.; Shu, G.Q.; Wei, H.Q.; Liang, X.Y. Theoretical research on working fluid selection for a high-temperature regenerative transcritical dual-loop engine organic Rankine cycle. *Energy Convers. Manag.* **2014**, *86*, 764–773. [[CrossRef](#)]
20. Dong, B.S.; Xu, G.Q.; Cai, Y.; Li, H.W. Analysis of zeotropic mixtures used in high-temperature Organic Rankine cycle. *Energy Convers. Manag.* **2014**, *84*, 253–260. [[CrossRef](#)]
21. Shu, G.Q.; Liu, L.N.; Tian, H.; Wei, H.Q.; Xu, X.F. Performance comparison and working fluid analysis of subcritical and transcritical dual-loop organic Rankine cycle (DORC) used in engine waste heat recovery. *Energy Convers. Manag.* **2013**, *74*, 35–43. [[CrossRef](#)]
22. Shu, G.Q.; Liu, L.N.; Tian, H.; Wei, H.Q.; Yu, G.P. Parametric and working fluid analysis of a dual-loop organic Rankine cycle (DORC) used in engine waste heat recovery. *Appl. Energy* **2014**, *113*, 1188–1198. [[CrossRef](#)]
23. Shu, G.Q.; Liu, L.N.; Tian, H.; Wei, H.Q.; Liang, Y.C. Analysis of regenerative dual-loop organic Rankine cycles (DORCs) used in engine waste heat recovery. *Energy Convers. Manag.* **2013**, *76*, 234–243. [[CrossRef](#)]
24. Zhang, H.G.; Wang, E.H.; Fan, B.Y. A performance analysis of a novel system of a dual loop bottoming organic Rankine cycle (ORC) with a light-duty diesel engine. *Appl. Energy* **2013**, *102*, 1504–1513. [[CrossRef](#)]
25. Yang, F.B.; Dong, X.R.; Zhang, H.G.; Wang, Z.; Yang, K.; Zhang, J.; Wang, E.H.; Liu, H.; Zhao, G.Y. Performance analysis of waste heat recovery with a dual loop organic Rankine cycle (ORC) system for diesel engine under various operating conditions. *Energy Convers. Manag.* **2014**, *80*, 243–255. [[CrossRef](#)]
26. Wang, E.H.; Zhang, H.G.; Zhao, Y.; Fan, B.Y.; Wu, Y.T.; Mu, Q.H. Performance analysis of a novel system combining a dual loop organic Rankine cycle (ORC) with a gasoline engine. *Energy* **2012**, *43*, 385–395. [[CrossRef](#)]
27. Wang, E.H.; Zhang, H.G.; Fan, B.Y.; Ouyang, M.G.; Yang, F.Y.; Yang, K.; Wang, Z.; Zhang, J.; Yang, F.B. Parametric analysis of a dual-loop ORC system for waste heat recovery of a diesel engine. *Appl. Therm. Eng.* **2014**, *67*, 168–178. [[CrossRef](#)]
28. Choi, B.C.; Kim, Y.M. Thermodynamic analysis of a dual loop heat recovery system with trilateral cycle applied to exhaust gases of internal combustion engine for propulsion of the 6800 TEU container ship. *Energy* **2013**, *58*, 404–416. [[CrossRef](#)]
29. Song, J.; Gu, C.W. Parametric analysis of a dual loop Organic Rankine Cycle (ORC) system for engine waste heat recovery. *Energy Convers. Manag.* **2015**, *105*, 995–1005. [[CrossRef](#)]
30. Song, J.; Gu, C.W. Performance analysis of a dual-loop organic Rankine cycle (ORC) system with wet steam expansion for engine waste heat recovery. *Appl. Energy* **2015**, *156*, 280–289. [[CrossRef](#)]
31. Yang, F.B.; Zhang, H.G.; Yu, Z.B.; Wang, E.H.; Meng, F.X.; Liu, H.D.; Wang, J.F. Parametric optimization and heat transfer analysis of a dual loop ORC (organic Rankine cycle) system for CNG engine waste heat recovery. *Energy* **2017**, *118*, 753–775. [[CrossRef](#)]
32. Lai, N.A.; Wendland, M.; Fischer, J. Working fluids for high-temperature organic Rankine cycles. *Energy* **2011**, *36*, 199–211. [[CrossRef](#)]

33. Braimakis, K.; Karellas, S. Exergetic optimization of double stage Organic Rankine Cycle (ORC). *Energy* **2018**, *149*, 296–313. [[CrossRef](#)]
34. Dai, X.Y.; Shi, L.; An, Q.S.; Qian, W.Z. Screening of hydrocarbons as supercritical ORCs working fluids by thermal stability. *Energy Convers. Manag.* **2016**, *126*, 632–637. [[CrossRef](#)]
35. Tsang, W. Thermal stability of cyclohexane and 1-hexene. *Int. J. Chem. Kinet.* **2010**, *10*, 1119–1138. [[CrossRef](#)]
36. And, W.C.A.; Bruno, T.J. Rapid Screening of Fluids for Chemical Stability in Organic Rankine Cycle Applications. *Ind. Eng. Chem. Res.* **2005**, *44*, 5560–5566.
37. Yang, F.B.; Zhang, H.G.; Song, S.S.; Bei, C.; Wang, H.J.; Wang, E.H. Thermoeconomic multi-objective optimization of an organic Rankine cycle for exhaust waste heat recovery of a diesel engine. *Energy* **2015**, *93*, 2208–2228. [[CrossRef](#)]
38. Li, J.; Liu, Q.; Ge, Z.; Duan, Y.Y.; Yang, Z.; Di, J.W. Optimized liquid-separated thermodynamic states for working fluids of organic Rankine cycles with liquid-separated condensation. *Energy* **2017**, *141*, 652–660. [[CrossRef](#)]
39. Li, J.; Liu, Q.; Duan, Y.Y.; Yang, Z. Performance analysis of organic Rankine cycles using R600/R601a mixtures with liquid-separated condensation. *Appl. Energy* **2017**, *190*, 376–389. [[CrossRef](#)]
40. Liu, Q.; Duan, Y.Y.; Yang, Z. Performance analyses of geothermal organic Rankine cycles with selected hydrocarbon working fluids. *Energy* **2013**, *63*, 123–132. [[CrossRef](#)]
41. Liu, Q.; Shen, A.J.; Duan, Y.Y. Parametric optimization and performance analyses of geothermal organic Rankine cycles using R600a/R601a mixtures as working fluids. *Appl. Energy* **2015**, *148*, 410–420. [[CrossRef](#)]
42. Ge, Z.; Wang, H.; Wang, H.T.; Wang, J.J.; Li, M.; Wu, F.Z.; Zhang, S.Y. Main parameters optimization of regenerative organic Rankine cycle driven by low-temperature flue gas waste heat. *Energy* **2015**, *93*, 1886–1895. [[CrossRef](#)]
43. Ge, Z.; Li, J.; Liu, Q.; Duan, Y.Y.; Yang, Z. Thermodynamic analysis of dual-loop organic Rankine cycle using zeotropic mixtures for internal combustion engine waste heat recovery. *Energy Convers. Manag.* **2018**, *166*, 201–214. [[CrossRef](#)]
44. Holland, J.H. *Adaptation in Nature and Artificial Systems: An Introductory Analysis with Applications to Biology, Control and Artificial Intelligence*; MIT Press: Cambridge, MA, USA, 1992.
45. Wang, E.H.; Zhang, H.G.; Fan, B.Y.; Wu, Y.T. Optimized performances comparison of organic Rankine cycles for low grade waste heat recovery. *J. Mech. Sci. Technol.* **2012**, *26*, 2301–2312. [[CrossRef](#)]
46. Xi, H.; Li, M.J.; Xu, C.; He, Y.L. Parametric optimization of regenerative organic Rankine cycle (ORC) for low grade waste heat recovery using genetic algorithm. *Energy* **2013**, *58*, 473–482. [[CrossRef](#)]
47. Wang, J.F.; Yan, Z.Q.; Wang, M.; Ma, S.L.; Dai, Y.P. Thermodynamic analysis and optimization of an (organic Rankine cycle) ORC using low grade heat source. *Energy* **2013**, *49*, 356–365. [[CrossRef](#)]
48. Imran, M.; Usman, M.; Park, B.S.; Kim, H.J.; Lee, D.H. Multi-objective optimization of evaporator of organic Rankine cycle (ORC) for low temperature geothermal heat source. *Appl. Therm. Eng.* **2015**, *80*, 1–9. [[CrossRef](#)]
49. Wang, J.F.; Yan, Z.Q.; Wang, M.; Li, M.Q.; Dai, Y.P. Multi-objective optimization of an organic Rankine cycle (ORC) for low grade waste heat recovery using evolutionary algorithm. *Energy Convers. Manag.* **2013**, *71*, 146–158. [[CrossRef](#)]
50. Wang, Y.Z.; Zhang, K.; Zheng, C.; CHne, H.Y. An Optimal Energy Management Method for the Multi-Energy System with Various Multi-Energy Applications. *Appl. Sci.* **2018**, *8*, 2273. [[CrossRef](#)]
51. Hong, Y.Y.; Yo, P.S. Novel Genetic Algorithm-Based Energy Management in a Factory Power System Considering Uncertain Photovoltaic Energies. *Appl. Sci.* **2017**, *7*, 438. [[CrossRef](#)]
52. Chen, H.J.; Goswami, D.Y.; Rahman, M.M.; Stefanakos, E.K. A supercritical Rankine cycle using zeotropic mixture working fluids for the conversion of low-grade heat into power. *Energy* **2011**, *36*, 549–555. [[CrossRef](#)]
53. Bao, J.J.; Zhao, L. A review of working fluid and expander selections for organic Rankine cycle. *Renew. Sustain. Energy Rev.* **2013**, *24*, 325–342. [[CrossRef](#)]

